 doi:10.1111/j.1365-2958.2010.07277.x

Biological and structural characterization of the *Mycobacterium smegmatis* nitroreductase NfnB, and its role in benzothiazinone resistance

Giulia Manina,[1,2,3†] Marco Bellinzoni,[2†] Maria Rosalia Pasca,[1†] João Neres,[3] Anna Milano,[1] Ana Luisa de Jesus Lopes Ribeiro,[1,4] Silvia Buroni,[1] Henrieta Škovierová,[5] Petronela Dianišková,[5] Katarína Mikušová,[5] Jozef Marák,[5] Vadim Makarov,[6] David Giganti,[2] Ahmed Haouz,[7] Anna Paola Lucarelli,[1] Giulia Degiacomi,[1] Aurora Piazza,[1] Laurent R. Chiarelli,[8] Edda De Rossi,[1] Elena Salina,[6] Stewart T. Cole,[3] Pedro M. Alzari[2] and Giovanna Riccardi[1]*

[1]*Dipartimento di Genetica e Microbiologia, Università degli Studi di Pavia, via Ferrata, 1, 27100 Pavia, Italy.*
[2]*Unité de Biochimie Structurale, CNRS-URA 2185, Institut Pasteur, 75724 Paris Cedex 15, France.*
[3]*Global Health Institute, Ecole Polytechnique Fédérale de Lausanne, CH-1015 Lausanne, Switzerland.*
[4]*DiSCAFF, Università del Piemonte Orientale, Via Bovio 6, 28100 Novara, Italy.*
[5]*Departments of Biochemistry and Analytical Chemistry, Faculty of Natural Sciences, Comenius University, Mlynska dolina, 84215 Bratislava, Slovakia.*
[6]*A. N. Bakh Institute of Biochemistry, Russian Academy of Science, 119071 Moscow, Russia.*
[7]*Plateforme de Cristallogenèse et Diffraction des Rayons X, Institut Pasteur, 75724 Paris cedex 15, France.*
[8]*Dipartimento di Biochimica 'A. Castellani', Università degli Studi di Pavia, via Taramelli, 3/b, 27100 Pavia, Italy.*

Summary

Tuberculosis is still a leading cause of death in developing countries, for which there is an urgent need for new pharmacological agents. The synthesis of the novel antimycobacterial drug class of benzothiazinones (BTZs) and the identification of their cellular target as DprE1 (Rv3790), a component of the decaprenylphosphoryl-β-D-ribose 2′-epimerase complex, have been reported recently. Here, we describe the identification and characterization of a novel resistance mechanism to BTZ in *Mycobacterium smegmatis*. The overexpression of the nitroreductase NfnB leads to the inactivation of the drug by reduction of a critical *nitro*-group to an *amino*-group. The direct involvement of NfnB in the inactivation of the lead compound BTZ043 was demonstrated by enzymology, microbiological assays and gene knockout experiments. We also report the crystal structure of NfnB in complex with the essential cofactor flavin mononucleotide, and show that a common amino acid stretch between NfnB and DprE1 is likely to be essential for the interaction with BTZ. We performed docking analysis of NfnB-BTZ in order to understand their interaction and the mechanism of nitroreduction. Although *Mycobacterium tuberculosis* seems to lack nitroreductases able to inactivate these drugs, our findings are valuable for the design of new BTZ molecules, which may be more effective *in vivo*.

Accepted 22 June, 2010. *For correspondence. E-mail giovanna.riccardi@unipv.it; Tel. (+39) 0382 985574; Fax (+39) 0382 528496.
†These authors contributed equally to this work.

Introduction

Tuberculosis (TB) is still a leading cause of death in developing countries, especially those of sub-Saharan Africa where TB is epidemic, partly because of the increased susceptibility caused by the widespread HIV prevalence in those populations (Maartens and Wilkinson, 2007). Moreover, the spread of multidrug-resistant (MDR-TB) and extensively drug-resistant (XDR-TB) strains of *Mycobacterium tuberculosis* has become a major clinical and public health problem (Matteelli *et al.*, 2007). The last 40 years have seen no new class of anti-TB drugs and, among the small number of compounds with antitubercular activity designed, only a few candidates, such as PA-824 and diarylquinolines, are currently undergoing clinical trials (Riccardi *et al.*, 2009).

We have recently discovered a novel and extremely effective antimycobacterial drug class, namely benzothiazinones (BTZs), that shows highly bactericidal activity *in vitro*, *ex vivo* and in the chronic-TB mouse model (Makarov *et al.*, 2009). The best available candidate among this class is the compound BTZ043 (Fig. 1),

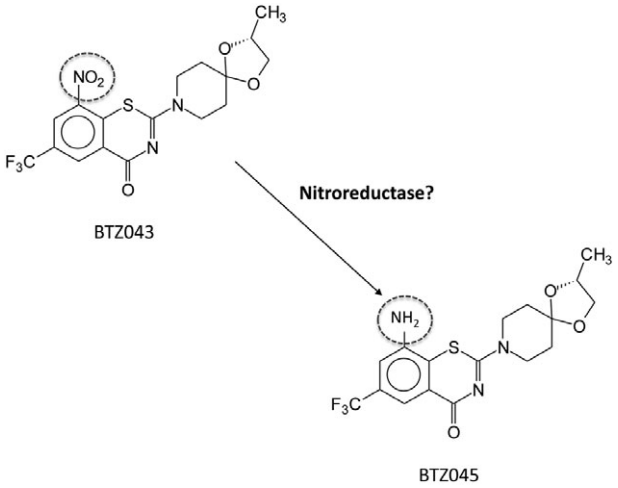

Fig. 1. Chemical formula of BTZ043 and the corresponding *amino*-compound BTZ045.

characterized by a *nitro*-group essential for its antimycobacterial activity (Makarov *et al*., 2009); its target has been demonstrated to be the enzyme decaprenylphosphoryl-β-D-ribose *2′*-epimerase, particularly its DprE1 component encoded by the *dprE1*/*Rv3790* gene (Makarov *et al*., 2009). This enzyme acts in concert with DprE2 (coded by the neighbouring *dprE2*/*Rv3791* gene) to convert decaprenylphosphoryl ribose (DPR) into decaprenylphosphoryl arabinose (DPA), a substrate for arabinosyltransferases in the synthesis of the mycobacterial cell wall arabinogalactan (AG) and lipoarabinomannan polysaccharides (Mikusova *et al*., 2005; Wolucka, 2008). Arabinogalactan is a fundamental component of the mycobacterial cell wall, which covalently binds the outer layer of mycolic acids to peptidoglycan (Wolucka, 2008). Indeed, both the *dprE1* and *dprE2* genes were predicted to be essential by *Himar*1-based transposon mutagenesis in *M. tuberculosis* H37Rv (Sassetti *et al*., 2003), thus validating both enzymes as targets for drug development.

The search for possible resistance mechanisms to BTZs showed that spontaneous missense mutations of Cys387 in DprE1, as well as the overexpression of the wild-type protein, confer high levels of resistance to BTZ043, in different mycobacterial species. We also demonstrated that BTZ043 can block the epimerization reaction from radiolabelled DPR into DPA *in vitro* using membrane preparations from either *Mycobacterium smegmatis* or *Mycobacterium bovis* BCG, but not from the corresponding mutant strains (Makarov *et al*., 2009).

In the course of preliminary structure activity relationship studies (SAR), we previously showed that the single stereoisomers BTZ043 (*S*) and BTZ044 (*R*), both carrying a *nitro*-group, were the most active molecules against mycobacteria, while the corresponding *amino*-derivatives BTZ045S (*S*) and BTZ045R (*R*) were significantly less active both in *M. smegmatis* and in *M. tuberculosis* (Fig. 1) (Makarov *et al*., 2009). This finding raised the question of whether mycobacterial nitroreductases (NRs) could be involved in inactivating the drug by reducing the *nitro*-forms to the corresponding *amino*-forms. NR encoding genes are in fact widespread among bacterial genomes, but are also found in eukaryotes. The common presence of NRs in bacteria may be ascribed to the fact that nitroaromatic compounds are often toxic and mutagenic, and several microorganisms have developed enzymatic pathways in order to degrade and detoxify such compounds (Roldán *et al*., 2008). Bacterial NRs belong to the Nitro_FMN_reductase superfamily and catalyse the reduction of nitrocompounds using NAD(P)H as electron donor in an obligatory two-electron transfer, utilizing non covalently bound FMN as cofactor. Members of this enzymatic family include NAD(P)H:FMN oxidoreductase, oxygen-insensitive nitroreductase, flavin reductase P, dihydropteridine reductase, NADH oxidase and NADH dehydrogenase (Roldán *et al*., 2008). The prototype prokaryotic nitroreductase is NfnB/NfsB from *Escherichia coli*; the ability of this enzyme to reduce the *nitro*- to the corresponding *amino*-group has led to its use in studies of anticancer chemotherapy, by activating pro-drugs that contain a *nitro*-group in antitumor agents (Parkinson *et al*., 2000).

In this work, by microbiological, genetic, biochemical and structural approaches, we describe the identification and characterization of NfnB from *M. smegmatis*, an NR able to specifically reduce the *nitro*-compound, BTZ043, to the *amino*-derivative, BTZ045 (Fig. 1). To date, no orthologous or paralogous NR, able to perform this conversion, has been found in *M. tuberculosis,* consistent with the very low minimal inhibitory concentrations (MICs) of the drug against sensitive- and MDR-*M. tuberculosis* strains (Makarov *et al*., 2009; Pasca *et al*., 2010). However, the identification of a mycobacterial NR able to inactivate the BTZ drugs could be key to understanding the mechanism of action of this class of molecules, and help to improve the future clinical use of these current compounds.

Results

Overexpression of nfnB *confers resistance to BTZ043 in* M. smegmatis

In our previous work we reported the isolation of spontaneous mutants of *M. smegmatis*-resistant to BTZs (Makarov *et al*., 2009). The majority of them had missense mutations in the same codon, encoding Cys387 in Rv3790 (DprE1), the cellular target of BTZs (Makarov

et al., 2009). In the present study, we focused our attention on the first of a different series of *M. smegmatis*-resistant mutants, named GM22, which showed a lower resistance level (16X-MIC) to BTZ043 (Table S1).

In contrast to the aforementioned mutants, this strain harboured neither mutations in *MSMEG_6382* nor in *MSMEG_6385*, the genes orthologous to *M. tuberculosis dprE1* and *dprE2* respectively. To identify the gene(s) responsible for the BTZ resistance phenotype, GM22 was transformed with a wild-type *M. smegmatis* cosmid library, and a selection for sensitivity to BTZ043 was carried out. A transformant colony characterized by a resistance decrease from 16X-MIC to 2X-MIC was isolated, and the cosmid, REP3, responsible for restoration of BTZ043 sensitivity, was isolated and partially sequenced; the cloned genomic fragment extended from nucleotides 6554151 to 6580426 (according to the *M. smegmatis* genome numbering from TIGR/JCVI). To confirm that this fragment was indeed responsible for the BTZ-sensitive phenotype, the GM22/REP3 strain was cured of the cosmid and the cured strain shown to display the original level of resistance to BTZ043, thus confirming the causal role of REP3.

Subcloning experiments of the cosmid REP3 were then performed and this led to the identification of a 4456 bp KpnI–SphI fragment. This genomic fragment contained, among others, the *MSMEG_6503* gene, coding for a putative transcriptional regulator from the TetR family, and the *MSMEG_6505* gene, which was annotated as *nfnB* due to its 35% sequence identity to the *E. coli* NfnB/NfsB nitroreductase (Fig. S1). Both genes were amplified from the *M. smegmatis* GM22 mutant and sequenced. The sequence analysis revealed no mutations in the *nfnB* gene of GM22 mutant, but a point mutation in *MSMEG_6503*. This mutation led to the substitution of Leu137 by Pro, leading to the hypothesis that the GM22 resistance could be due to a defective repressor (MSMEG_6503), possibly causing overexpression of NfnB and, consequently, the reduction of the BTZ *nitro*-molecule to its less active *amino*-derivative. *Vice versa*, the restored BTZ043 sensitivity in the GM22 complemented mutant could be due to the presence of several copies of the wild-type allele of *MSMEG_6503* from the REP3 cosmid. Consistent with this hypothesis, the MIC of BTZ045, the *amino* derivative of BTZ043, for *M. smegmatis* was already known to be 0.5 μg ml^{-1} versus 4–8 ng ml^{-1} of the original *nitro* compound (Makarov *et al*., 2009).

Moreover, 14 other spontaneous mutants, showing different levels of resistance (8–32X-MIC), were found to carry mutations in the *MSMEG_6503* gene, including deletions (AL43, AL45, AL47, AL49, AL50, AL51, AL53, AL54, AL57 mutants) and insertions (AL46 mutant) (Fig. S2, Table S1). All the mutant strains were predicted to produce a truncated form of the protein. One of these mutants, AL55, presents a mutation in the hypothetical repressor binding site (Fig. S2).

To validate this hypothesis, the wild-type *MSMEG_6503* gene from the REP3 cosmid was cloned into the constitutive expression vector pSODIT-2. When the recombinant plasmid was transformed into *M. smegmatis* GM22, the wild-type sensitivity to BTZ043 was restored (data not shown). This result suggested that the overexpression of *nfnB* could represent a specific mechanism of resistance to BTZ043 in *M. smegmatis*.

The MSMEG_6503 regulator binds two conserved palindromic sites in the MSMEG_6503-nfnB *intergenic region*

To analyse the transcription of *nfnB* and *MSMEG_6503* genes, the 5′ end of the two transcripts was mapped by 5′-RACE experiments (Fig. 2). The sequence upstream of the transcriptional start sites revealed the presence of hypothetical −10 and −35 promoter regions (boxed in Fig. 2) for both genes. Two conserved sequences palindromic with respect to one another were observed in the 90bp *MSMEG_6503-nfnB* intergenic region (highlighted in grey in Fig. 2). The first one overlapped the *MSMEG_6503* promoter region, while the second was localized just downstream of the *nfnB* transcriptional start site. To verify the role of MSMEG_6503 in *nfnB* regulation, MSMEG_6503 proteins from *M. smegmatis* mc^{2}155 (Fig. S3) and GM22 were purified and used in DNA binding assays. A fragment of 190bp, containing the *MSMEG_6503-nfnB* intergenic region was obtained by PCR with the primers nfnBinF and nfnBinR (Table S2) and used as a probe. As shown in Fig. 3, MSMEG_6503 from

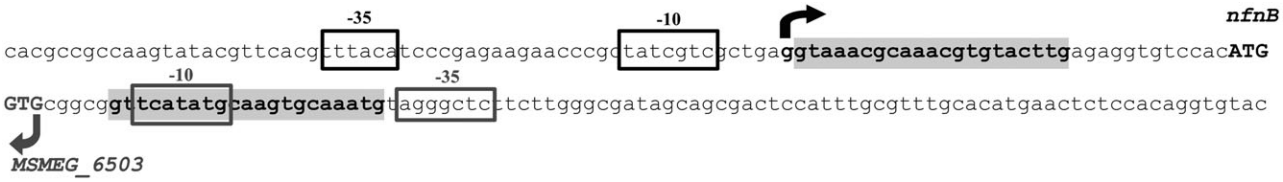

Fig. 2. Organization of the *MSMEG_6503-nfnB* intergenic region. Translational start codons are in bold capital letters; transcriptional start sites are in bold and indicated by an arrow; −35 and −10 promoter regions are boxed; hypothetical MSMEG_6503 binding sites are shaded in grey; all the elements of *MSMEG_6503* are indicated in grey, while those of *nfnB* in black.

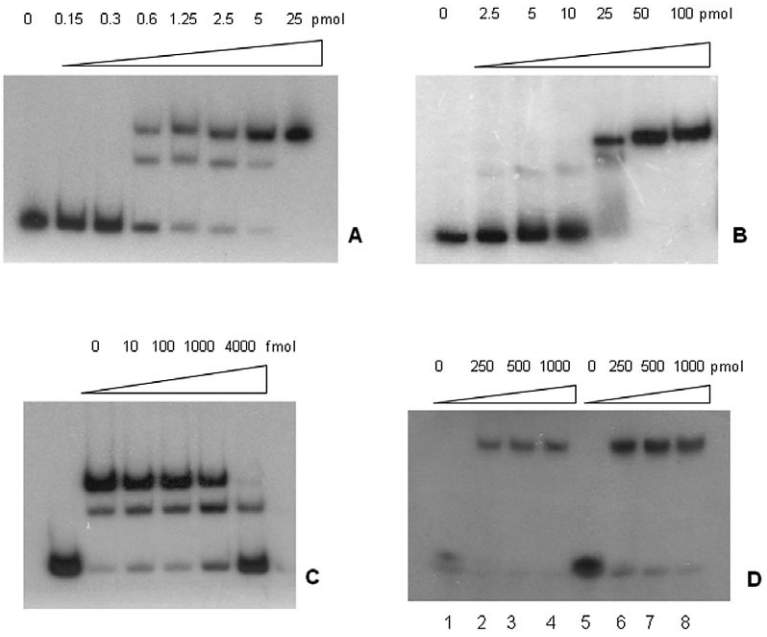

Fig. 3. DNA binding of MSMEG_6503 from *M. smegmatis* wild-type and mutant strains. Approximately 10 fmol of a 190 bp fragment was assayed with different amounts of MSMEG_6303 wild-type (A) and mutated (B) purified proteins. Different amounts of unlabelled probe (expressed in fmol) were assayed with MSMEG_6303 wild-type (2.5 pmol) and 10 fmol of labelled fragment (C). Binding of MSMEG_6303 wild-type protein on Box7/Box8 (*MSMEG_6503* upstream palindrome) (lanes 1–4) and Box9/Box10 (*nfnB* upstream palindrome) (lanes 5–8) is shown (D). The quantity of repressor per sample is expressed in pmol.

M. smegmatis mc^{2}155 was able to bind and efficiently retard this region (Fig. 3A), while the mutant protein bound less efficiently, as the same effect was only observed with a 10-fold excess of protein (Fig. 3B). The specificity of the protein-DNA interaction was confirmed by the ability of cold competitor DNA to reverse the mobility shift (Fig. 3C). Moreover, to better define the MSMEG_6503 binding sequence, Box7 and Box8 oligos, corresponding to the *MSMEG_6503* upstream palindrome, and Box9 and Box10, corresponding to the *nfnB* upstream palindrome, were labelled and used as probes in binding assays. The data clearly demonstrated that the purified wild-type protein was able to efficiently retard these regions (Fig. 3D), strongly suggesting their role as operator sites for the MSMEG_6503 regulator.

Overexpression of nfnB *confers resistance to BTZ043 in different mycobacterial species*

In order to verify whether BTZ043 resistance in *M. smegmatis* GM22 mutant was associated with overexpression of NfnB, the *nfnB* gene was cloned into pSODIT-2, and both wild-type *M. smegmatis* and *M. tuberculosis* H37Rv strains were transformed with the recombinant construct and the empty pSODIT-2 vector as control. As shown in Table 1, the *M. smegmatis* strains overproducing NfnB showed a 16-fold increase of the resistance level to BTZ043, comparable with the resistance observed for the GM22. Also in *M. tuberculosis*, overexpression of *M. smegmatis* NfnB conferred an eightfold increase in resistance to BTZ043.

Real-time PCR (RT-PCR) was then performed on RNA extracted from wild-type *M. smegmatis* and some mutant strains in the absence of the drug (Table 2). A 390 (± 56)-fold increase in transcription of *nfnB* in GM22 with respect to the wild-type parent was observed. As shown in Table 2, higher levels of *nfnB* expression were detected in AL49 (characterized by a 11 bp deletion in the *MSMEG_6503* coding region) and in AL55 (which has a mutation in the MSMEG_6503 binding site). A similar *nfnB* expression level was found in *M. smegmatis* strain transformed with pSODIT-2/*nfnB* (Table 2). Moreover, overex-

Table 1. *nfnB* overexpression confers BTZ043 resistance both in *M. smegmatis* and *M. tuberculosis*.

	BTZ043 MIC (ng ml^{-1})	
Plasmids	*M. smegmatis*	*M. tuberculosis*
pSODIT-2	4	1.5
nfnB/pSODIT-2	64	12

Table 2. *nfnB* and *MSMEG_6503* expression levels by RT-PCR in different *M. smegmatis* strains.

M. smegmatis strains	*nfnB*	*MSMEG_6503*
mc^{2}155	1	1
GM22	390 ± 56	3.01 ± 0.1
AL49	788 ± 42	30 ± 3
AL55	410 ± 28	29 ± 5
pSODIT-2/mc^{2}155	1	n.d.
nfnB/pSODIT-2/mc^{2}155	296 ± 30	n.d.

n.d., not determined.

Table 3. BTZ043 MIC variation in *M. smegmatis* wild-type, GM22 mutant and *nfnB* deleted strains.

	MIC in *M. smegmatis*			
Compounds	mc²155	Δ*nfnB* mc²155	GM22	Δ*nfnB* GM22
BTZ043 (ng ml⁻¹)	4	4	16	4
Rifampicin (μg ml⁻¹)	1	1	1	1

pression of the repressor encoding gene *MSMEG_6503* was detected in all the mutants analysed (Table 2). In the case of GM22 and AL49 the protein produced is mutated and with a reduced affinity for its recognition site; in mutant AL55 the repressor is in the wild-type form but there is a mutation in the binding site.

The results unambiguously showed that *nfnB* was strongly overexpressed in GM22, AL49 and AL55, indicating that the mutated MSMEG_6503 repressor did not efficiently repress the transcription of *nfnB*, due to its lower affinity for the operator region (Fig. 2). The presence of BTZ043 did not significantly affect the expression of *nfnB* in the wild-type strain, as cultures grown with the drug revealed about twofold repression compared with cultures grown in its absence (data not shown).

Deletion of nfnB *decreases resistance of GM22 mutant to BTZ043*

To further confirm the direct role of NfnB in *M. smegmatis* GM22 resistance to BTZ043, an in-frame unmarked deletion was created in the *nfnB* gene through a two-step homologous recombination (Parish and Stoker, 2000). As shown in Table 3, the Δ*nfnB* strain of GM22 has a restored wild-type phenotype, corroborating the function of NfnB in BTZ043 resistance. On the contrary, no MIC decrease was observed in the Δ*nfnB* strain of mc²155 compared with the wild-type strain. This can be explained on the one hand by the remarkable potency of BTZ043 and its very low MIC value and, on the other, by the wild-type regulator *MSMEG_6503* efficiently inhibiting *nfnB* expression. The MIC assessment was conducted in parallel with rifampicin as a control drug, and all the strains tested showed the same susceptibility (Table 3).

GM22 mutant converts BTZ043 to BTZ045 faster than wild-type M. smegmatis

Both wild-type *M. smegmatis* and GM22, overexpressing *nfnB*, were evaluated for their ability to convert the *nitro*-compound (BTZ043) to the *amino*-derivative (BTZ045), by high-pressure liquid chromatography (HPLC) analysis of culture media. GM22 transforms the *nitro*- to the *amino*-compound more efficiently and more rapidly compared with *M. smegmatis* (Table 4a, Fig. S4). Indeed, the mutant strain was able to reduce 70% of BTZ043 into BTZ045 after 3 h growth. Similar results were also achieved with wild-type *M. smegmatis* transformed with *nfnB*/pSODIT-2 recombinant plasmid (data not shown), thus confirming our hypothesis. In order to verify if BTZ addition was able to inhibit cell growth in the wild-type strain with respect to the resistant mutant, cell counting was performed. A small comparable reduction in cell viability was observed in GM22 and wild-type strains (data not shown). These findings are consistent with a role for NfnB in reduction of the active BTZ043 to the inactive BTZ045.

BTZ043 increases NAD(P)H oxidase activity of NfnB

NfnB from *M. smegmatis* is a 25.5 kDa enzyme which, as mentioned above, was annotated as a putative FMN-dependent nitroreductase on the basis of its sequence similarity with other bacterial nitroreductases, including *E. coli* NfnB/NfsB. A ClustalW analysis was thus performed between the two primary sequences. The two enzymes show significant similarity at the N-terminal end (Fig. S1), specifically between Arg25 and Arg72 (NfnB numbering) that define the hypothetical FMN-binding region.

The *M. smegmatis* enzyme was successfully expressed as a His_6-tagged form in *E. coli*, with final yields reaching 100 mg of purified protein from 20 g of wet cell biomass (Fig. S5). The purified enzyme was yellow in all purification steps, suggesting the presence of a flavin coenzyme, most likely in the oxidized state; this was confirmed by UV-Vis spectroscopy (data not shown). A kinetic analysis was then carried out using *E. coli* NfsB as an internal control. The optimal pH determined for NfnB activity ranged from 7.5 to 9.0; NfnB and NfsB had comparable

Table 4a. BTZ043 to BTZ045 transformation in *M. smegmatis* cultures.

	1 h growth	3 h growth
M. smegmatis	BTZ043:BTZ045	BTZ043:BTZ045
mc²155	90:10	80:20
GM22	50:50	30:70

Table 4b. BTZ043 to BTZ045 transformation in *M. tuberculosis* cultures.

	6 h growth	18 h growth	72 h growth
M. tuberculosis	BTZ043:BTZ045	BTZ043:BTZ045	BTZ043:BTZ045
H37Rv	99:1	94:6	80:20

Table 5. Kinetic parameters for NfnB from *M. smegmatis* versus NfsB from *E. coli*.

	K_m (μM)	K_{cat} (min^{-1})
M. smegmatis		
NADH	10.75 ± 0.21	4.20 ± 0.14
NADPH	8.15 ± 0.21	4.32 ± 0.15
E. coli		
NADH	6.68 ± 1.38	13.08 ± 1.47
NADPH	9.9 ± 1.68	14.5 ± 0.49

NAD(P)H-oxidase activities, indicating that NfnB does not have a strong preference for either NADH or NADPH as the electron donor (Table 5). Moreover, addition of micromolar amounts of BTZ043 to the assay mixture led to a significant increase in the rate of NADPH oxidation. In contrast, when five other potential substrates, chosen among the reported substrates of other bacterial nitroreductases (namely quinone menadione, nitrofurazone, methyl 4-nitrobenzoate, 4-nitrobenzene methyl sulfonate, and 4-nitroacetophenone) (Zenno *et al.*, 1996) were tested, no detectable effects on the NADPH-oxidase activity of NfnB were observed (data not shown). These results suggested that NfnB has a relative specificity for BTZ molecules, although the physiological substrate(s) remain to be identified.

BTZ043 is a substrate of NfnB

In order to assess the activity of the purified NfnB protein towards BTZ043, an indirect evaluation was initially performed, using an assay in which BTZ043 blocks the epimerization of DPR to DPA (Makarov *et al.*, 2009). Recombinant NfnB enzyme was thus added to the assay mixtures to monitor DPA synthesis from its precursor 5-phosphoribose diphosphate (pRpp) in *M. smegmatis* membranes, to evaluate whether its presence had any detectable effect on the inhibition of the epimerization of DPR to DPA by BTZ043. In the absence of BTZ043, DPA production was detected (Fig. 4, lane 1) and its synthesis was not affected by the addition of the pure NfnB protein (Fig. 4, lane 2); in presence of BTZ043, DPA synthesis was inhibited at the stage of DPR (Fig. 4, lane 3), suggesting that the drug was inhibiting *M. smegmatis* DprE1 (MSMEG_6382). When BTZ043 was pretreated with purified NfnB prior to addition to the reaction mixture, DPA was still formed (Fig. 4, lane 4), most likely due to the conversion of the active drug (BTZ043) to its inactive amino form. In order to evaluate this case we examined the composition of the pre-incubated BTZ043-NfnB reaction mixture by LC-MS. We found out that the peak area corresponding to BTZ043 (m/z 432) in this sample decreased to 46% of the total peak area (Fig. S6, Panel A) from 97% found in the controls without NADH (Fig. S6B), or without NfnB (Fig. S6C). The expected product of the reaction, BTZ045 (m/z 402), presented 17% of the total peak area, while the intermediates of the reaction, namely the nitroso (m/z 416) and the hydroxylamine forms (m/z 418), comprised 7% and 30% of the total peak area respectively (Fig. S6A). The reduction of BTZ043 by NfnB most likely proceeds in the final reaction mixture, since a significant reduction of the BTZ043 effect on DPR epimerization in presence of added NfnB was observed (Fig. 4, lane 4). These data confirmed that NfnB is able to reduce and inactivate BTZ043.

In order to verify the scope of NfnB and its possible involvement in the metabolism of other drugs, we investigated whether NfnB could also reduce the nitro group of PA-824. PA-824 is a bicyclic nitroimidazole that has potent activity against *M. tuberculosis* and is a promising candidate for TB treatment, currently undergoing clinical trials. Using the resazurin reduction assay, we confirmed that *M. smegmatis* is naturally resistant to PA-824 as reported previously (Stover *et al.*, 2000). Consequently, NfnB could be responsible for the lack of activity of this compound against *M. smegmatis*.

Using the LC-MS method, we verified that PA-824 is indeed reduced by NfnB, first to its hydroxylamine analogue, which subsequently decomposes to a metabolite lacking the imidazole ring, as described by Singh and colleagues (2008). Contrary to what was observed in *M. tuberculosis*, the des-nitro metabolite (major metabolite of PA-824 formed in TB with release of toxic nitrous acid) was not detected in the NfnB-mediated reduction of PA-824, in agreement with our hypothesis. However, the *M. smegmatis nfnB*-knockout mutant was equally resistant to PA-824 as the wild-type strain (data not shown), pointing to additional mechanisms underlying the natural resistance of *M. smegmatis* to this drug.

M. tuberculosis *may lack NRs or NR-like enzymes able to inactivate BTZ drugs*

The involvement of NfnB in BTZ-resistance in *M. smegmatis* naturally raises the question of whether one or

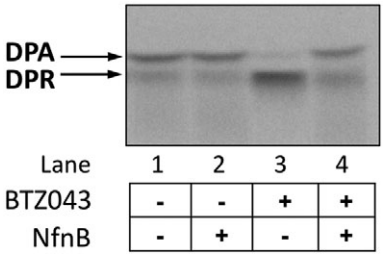

Fig. 4. TLC analysis of DPA/DPR produced in the cell-free assay in presence/absence of recombinant NfnB. The presence/absence of BTZ043 and NfnB is indicated by +/–. The bands corresponding to DPR and DPA are indicated by arrows.

Table 6. Crystallographic data collection and refinement statistics.

	SeMet SAD	Native	NADPH complex
Data collection			
Beamline	Soleil Proxima-1	Soleil Proxima-1	ESRF ID23-2
Resolution (Å)	34.6–2.5 (2.57–2.50)	44.2–1.75 (1.84–1.75)	59.8–1.80 (1.90–1.80)
Wavelength (Å)	0.9790	1.0332	0.8726
Space group	$I\,2_12_12_1$	$I\,2_12_12_1$	$I\,2_12_12_1$
Unit-cell parameters *a, b, c* (Å)	85.23, 115.26, 118.92	85.19, 114.97, 118.90	85.55, 115.61, 119.58
Multiplicity	2.6 (2.6)	3.7 (3.7)	3.7 (3.7)
Completeness (%)	97.4 (98.2)	99.7 (99.4)	100.0 (99.9)
R_{merge}[a]	0.106 (0.401)	0.070 (0.464)	0.101 (0.464)
No. of unique reflections	38161 (2849)	58860 (8451)	55133 (7971)
$\langle I/\sigma(I)\rangle$	8.8 (3.0)	13.3 (3.1)	9.5 (3.0)
Refinement statistics			
No. of reflections used	–	55863	52318
R_{work}[b]	–	0.151	0.149
R_{free}[b]	–	0.174	0.173
RMSD from ideal			
Bond lengths (Å)	–	0.010	0.010
Angles (°)	–	0.92	0.93
B factors (Å^2)	–		
Average	–	23.7	23.0
Protein	–	22.5	21.8
Waters	–	35.1	32.7
PDB entry	–	2WZV	2WZW

Values in parentheses refer to the outer (highest resolution) shell.

a. $R_{merge} = \sum_{hkl}\sum_{i}|I_i(hkl) - I(hkl)| \Big/ \sum_{hkl}\sum_{i} I_i(hkl)$.

b. $R = \sum_{hkl}|F(h)obs - F(h)calc| \Big/ \sum_{hkl} F(h)obs$; R_{free} calculated for 5% of the reflections, not used at any stage of structural refinement.

RMSD, root-mean-square-deviation.

more NR could be involved in BTZ resistance in *M. tuberculosis.* Although no orthologue of NfnB is present in the *M. tuberculosis* genome (http://tuberculist.epfl.ch/), nine hypothetical nitroreductases are predicted: Acg, Rv0306, MoeY, Rv2337c, FbiB, Rv3131, Rv3127, Rv3368c (Purkayastha *et al*., 2002) plus Rv3547, a nitroimidazo-oxazine specific nitroreductase, essential for the activation of the pro-drug PA-824 (Manjunatha *et al*., 2006; Singh *et al*., 2008). Furthermore, three other proteins homologous to Rv3547 can be identified, i.e. Rv1558, Rv1261c and Rv3178 (Singh *et al*., 2008), in addition to the lipoamide dehydrogenase LpdC (Rv0462), whose homologue in *M. smegmatis* has been shown to have some activity on non physiological substrates, including nitroheterocyclic compounds (Marcinkeviciene and Blanchard, 1997).

The genes *acg*, *Rv0306*, *moeY*, *fbiB*, *Rv3131*, *Rv3127*, *Rv3368c*, *Rv3547*, *Rv1558*, *Rv1261c*, *Rv3178* and *lpdC* were cloned into pSODIT-2 expression vector, while *Rv2337c* gene was cloned with its own promoter region into pMD31 vector. All the recombinant clones were transformed into *M. smegmatis* and *M. tuberculosis*, and the MIC was evaluated both aerobically and anaerobically, as it is known that some bacterial NRs, including NfsB, need anaerobic conditions to reduce nitroaromatic compounds (Linwu *et al*., 2009). None of the different *M. tuberculosis* NR had any effect on the MIC of BTZ043 in both species, irrespective of the conditions tested (Table S3). Control experiments revealed expression of all the hypothetical NRs (data not shown). In contrast, overexpression of NfnB conferred resistance to BTZ043 in both species but only under aerobic conditions (Table 1 and Table S3), indicating that NfnB is an oxygen-dependent NR as far as the reduction of BTZ043 is concerned. Overall, these data, as well as direct assessment by HPLC of the transformation of BTZ043 to BTZ045 in cultures of *M. tuberculosis* (Table 4b, Fig. S7), suggest that *M. tuberculosis* most probably lacks enzymes able to inactivate BTZ043 either in aerobic or anaerobic environment, consistent with the low MIC values of BTZ043 in *M. tuberculosis* and the fact that all the BTZ-resistant mutants isolated so far in this species harboured mutations in the target gene *dprE1*.

Crystal structure of NfnB and docking prediction of the NfnB-BTZ043 complex

The crystal structure of NfnB was determined at 1.75 Å resolution to final $R = 15.1\%$, $R_{free} = 17.4\%$ (Table 6). The enzyme adopts an homodimeric fold that does not deviate significantly from already known FMN-dependent nitro-

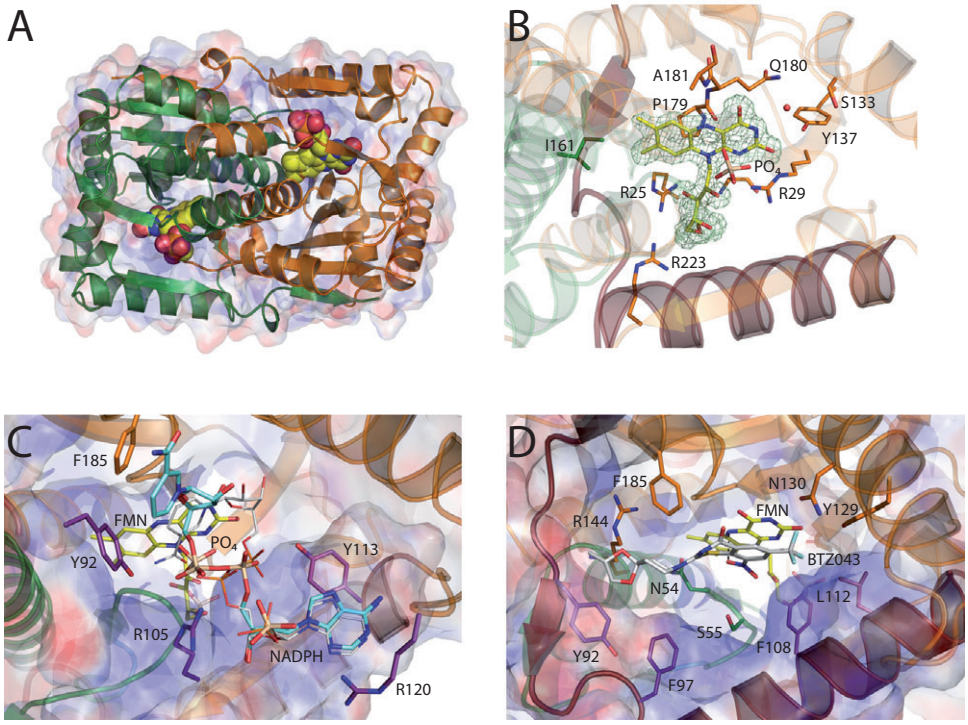

E

```
 86 VTVDFPYREGL--FQGVLQERRADFGSRLYAA 115 NfnB
    + VDFP ++GL  F   L  R  +FG RLY A
386 ICVDFPIKDGLGKFVSELDRRVLEFGGRLYTA 417 DprE1
```

Fig. 5. Structure of *M. smegmatis* NfnB and complexes with NADPH (experimental) and BTZ043 (predicted by docking).
A. Global fold of the homodimer of NfnB; the FMN prosthetic group is shown as 'Van der Waals' spheres. The protein surface, shown on the background, is coloured according to its electrostatic potential.
B. View of the FMN molecule and its co-ordinating residues. The sigma-A weighted difference electron density map (mF_o-DF_c), calculated before FMN was added to the model and contoured at the 3σ level, is shown in green. The region of the protein homologous to Rv3790 [alignment shown in (E)] is depicted in red. Note the inorganic phosphate ion in front of the isoalloxazine ring.
C. Close view of the NADPH molecule (sticks, carbon atoms in light blue) complexed to NfnB. The docking prediction for the same molecule in which the nicotinamide group stacks parallel to FMN is shown as thinner sticks (carbon atoms grey). Side-chains interacting with NADPH are also depicted as sticks, coloured ruby if they belong to the amino acid stretch homologous to DprE1 [shown in (E)]. The electrostatic surface of the protein, in background, is enhanced for the DprE1-like portion in NfnB.
D. Docking prediction of the BTZ043 binding (grey) into the NfnB active site. Amino acid side-chains are depicted as in (C).
E. Amino acid sequence alignment (ClustalW) of NfnB and DprE1, limited to the region (30 residues) displaying significant sequence similarity (see text).

reductases, i.e. the prototype NfsB from *E. coli* (Fig. 5A); the closest structural homologue according to both SSM (Krissinel and Henrick, 2004) and DALI (Holm *et al*., 2008) is an uncharacterized FMN-nitroreductase from *Bartonella henselae* (pdb entry 3GR3), with an overall RMSD between Cα atoms of 1.4 Å. The enzyme core is composed of a central five-stranded β-sheet, made by four antiparallel β-strands plus a fifth one (parallel to the first) contributed by the C-terminal residues of the opposite monomer; the β-sheet is flanked by two helices on the internal side, involved in dimerization, and three helices on the external one.

The active site is located at the interface of the dimer, and residues from both monomers indeed contribute to the non-covalent binding of FMN (Fig. 5B). As seen in other nitroreductases, a number of hydrogen bonds involving the isoalloxazine ring make it deviate from planarity. This distortion, known as 'butterfly bending', results in a ~165° angle between the pyrimidine and the dimethylbenzene rings and is consistent with an oxidized state of the FMN prosthetic group, as observed, among others, in *E. coli* NfsB (Lovering *et al*., 2001; Race *et al*., 2005) and *Enterobacter cloacae* NR (Haynes *et al*., 2002). On the opposite side (*re* face) of the flavin, some tetragonal-shaped residual density was modelled as a phosphate ion from the crystallization buffer (Fig. 5B). The proximity of the phosphate to the reactive portion of FMN suggests that this ion could be mimicking the position of the *nitro*-group of the substrate, an hypothesis supported by the consistent superimposition of this phosphate ion to

an acetate ion observed in the crystal structures of both the *E. coli* (Race *et al*., 2005) and *E. cloacae* enzymes (Haynes *et al*., 2002).

The structure of NfnB in complex with NADPH was obtained by the prior addition of the cofactor during crystallization, and was refined in the same crystallographic space group at 1.80 Å resolution to final $R = 14.9\%$, $R_{free} = 17.3\%$ (Table 6; Fig. 5C). The purine ring of the adenosine moiety stacks between the side-chains of Tyr113 and Arg120, while the 2′-phosphate group points externally making only a salt bridge with Arg105, which may explain why NfnB does not show significant specificity for either NADPH or NADH. Moreover, the nicotinamide moiety, which stacks parallel to the side-chain of Phe185, does not make electrostatic contacts and thus appears mobile; it is noteworthy that the amide group points outwards from the active site, most likely because this is still occupied by a phosphate ion in front of FMN (Fig. 5C). To confirm whether the observed binding mode of NADPH could be otherwise compatible with the hydride transfer to FMN, a docking calculation was made for NADPH restraining the co-ordinates of the adenosine moiety to the experimental ones. The solution with the lowest energy showed indeed the nicotinamide entering the active site and stacking approximately parallel to the isoalloxazine ring (Fig. 5C), suggesting that the observed NADPH binding mode is compatible with the formation of a productive complex.

All attempts to determine the crystal structure of NfnB in complex with any of the available BTZ derivatives, either by soaking or cocrystallization, were unsuccessful. Computational docking was therefore used to model the interaction between the enzyme and the lead compound BTZ043. As an assessment of the docking protocol, several structures of FMN-dependent nitroreductases complexed to small molecules were inspected, and six structures of *E. coli* NfsB with different ligands were retrieved for further analysis (pdb entries 1ICR, 1ICU, 1IDT, 1OO6, 1OON, 1OOQ, 1YKI) (Johansson *et al*., 2003; Race *et al*., 2005). The inspection of these structures suggested a common substrate binding mode: with the exceptions of the smallest molecules nicotinic acid and nitrofurazone, the other compounds were all positioned with their nitrobenzene moiety stacking parallel to the FMN isoalloxazine ring and the *nitro*-group pointing at ~ 3.5 Å to the reactive N5 of FMN. The position of the oxygen atoms of the *nitro*-group of these molecules coincides with that of two oxygens from the phosphate ion in front of FMN in NfnB (Fig. 5B). In order to maintain the BTZ043 molecule in an orientation compatible with the reaction, we therefore decided to restrain its *nitro*-group, during our calculations, in the position occupied by the phosphate ion in the experimental structure. To validate this assumption, the 5-(aziridin-1-yl)-2,4-dinitrobenzamide ligand in pdb entry 1IDT was redocked into the NfsB apo structure and the resulting complex indeed reproduced the deposited structure (data not shown).

The analysis of solvent-accessible surfaces in NfnB showed a larger substrate binding pocket for one of the monomers (~ 216 $Å^3$ for the pocket defined by chain B in pdb entry 2WZV). The symmetric pocket formed by the opposite monomer is smaller due to the different conformation of the main chain for residues Tyr92-Gln98, packed closer to the core of the enzyme. Since this loop appears as mobile in both chains, and its conformation differs due to distinct crystal packing constraints, the largest binding site was chosen as the pocket for docking. The best prediction of the NfnB-BTZ043 complex, in terms of free energy, is illustrated in Fig. 5D. As expected, the predicted orientation of the BTZ molecule places the nitrobenzene moiety into a parallel stacking with the isoalloxazine ring, where the *nitro*-group is expected to be kept in place by the interaction with Asn54 and Ser55. It is worth noting that this conformation, in addition to be consistent with the reaction, shows a remarkable surface complementarity of the substrate binding pocket of NfnB with the remainder of the BTZ molecule (Fig. 5D).

Discussion

There has been increased interest in bacterial NRs in the last few years due to their potential environmental and clinical applications, most notably for their usefulness in cancer therapy for prodrug activation (Roldán *et al*., 2008). In this study, we investigated the role of a nitroreductase in the metabolism of the antitubercular drug candidate, BTZ043, which targets the enzyme DprE1, essential for the biosynthesis of AGs and thus for the integrity of the mycobacterial cell wall (Makarov *et al*., 2009). In particular, we demonstrated that the overexpression of the FMN-dependent nitroreductase NfnB in *M. smegmatis*, driven by spontaneous mutations in the transcriptional repressor controlling its expression, is a novel BTZ resistance mechanism, involving drug inactivation, besides the already documented amino acid substitution on Cys387 of DprE1 (Makarov *et al*., 2009). Moreover, a recent report has shown that compounds from the dinitrobenzamide class also target DprE1 and that the same amino acid substitution in the target (C387G) confers dinitrobenzamide resistance (Christophe *et al*., 2009). As a nitroaromatic group is essential for the antimycobacterial activity of these compounds, similarly to BTZs (Christophe *et al*., 2009), the possible development of resistance due to the overexpression of a nitroreductase is an issue that should be considered.

The direct role of NfnB in BTZ inactivation has been confirmed both genetically, as the deletion of *nfnB* in the GM22 mutant restores a wild-type phenotype, as well as

biochemically, since BTZ043 was unambiguously shown to be a substrate of NfnB in cell free enzymatic assays. In order to further investigate the specific nitroreductase activity of NfnB, to better understand the metabolic fate of BTZ043 both in mycobacteria and in the host, and, eventually, to design new molecules resistant to inactivation, we carried out a biochemical and structural study of the enzyme.

Although the structure of NfnB shows the overall conservation of the enzyme fold with respect to the already known FMN-dependent nitroreductases (more than 60 homologous structures are available in the protein data bank), an interesting observation comes from the comparison of the primary sequences of NfnB and DprE1. An amino acid sequence alignment shows a common amino acid stretch of 30 amino acids between NfnB (residues 86–115) and DprE1 (residues 386–417), displaying 46% sequence identity (59% similarity) (Fig. 5E). It is noteworthy that this amino acid stretch is located at the C-terminal end of DprE1, the same region in which spontaneous mutations conferring resistance to BTZ were identified (Makarov *et al*., 2009), suggesting that this polypeptide portion might also play a key role in defining the relative specificity of NfnB towards the nitromolecules from the BTZ class. This portion of NfnB makes a long loop followed by an α-helix folding over the FMN site, where it contributes to the geometry of the active site and hence may be crucial in defining the specificity of the enzyme towards the substrate(s).

This hypothesis is supported by the predicted NfnB-BTZ043 complex, which indeed shows that several residues from this patch (namely Tyr92 and Phe97) are expected to interact with the drug, forming a pocket that binds the distal part of the molecule (Fig. 5D); the same region of the protein is also involved in binding NADPH, as proven experimentally (Fig. 5C). Furthermore, this region structurally deviates from the homologues (such as NfsB) more than the core of the protein and displays higher mobility, possibly related to flexibility in accommodating the substrate(s), as reflected by the average B factors in both the free enzyme and the complex with NADPH (averaged B for residues 92–98 from the two models is 37.3 $Å^2$ for chain A and 58.0 $Å^2$ for chain B, versus 22.2 $Å^2$ for the whole protein). This may, at least in part, explain the relative specificity of NfnB towards the BTZ molecules, as well as the failure to detect activity with canonical nitroreductase substrates. Moreover, the predicted binding mode of BTZ043 suggests that bigger substitutions at the distal site from the reactive *nitro*-group might render BTZs resistant to inactivation, even though (for the same reasons) they could lower the affinity for DprE1 or even abolish the interaction with the target. A careful evaluation of the effectiveness of any new BTZ compound, both *in vitro* and *in vivo*, may clarify this issue.

We also investigated whether *M. tuberculosis* possesses any nitroreductases able to carry out the same drug inactivation process. Although no NfnB homologue is present in *M. tuberculosis* genome, a total of 13 putative nitroreductases could be identified; none of these confers resistance to BTZ043 when overexpressed. These findings are consistent with the lower MIC in *M. tuberculosis* (1 ng ml^{-1}) compared with *M. smegmatis* (4 ng ml^{-1}), although other factors such as differences between the two species in the membrane permeability or in the affinity of DprE1 for the drug (due to the active site architecture) may contribute to explain the different MIC values. However, it has also been observed that the *nitro*-BTZ compounds are transformed into the corresponding *amino*-derivatives not only in *M. smegmatis* cultures overexpressing NfnB, but also in blood and urine from treated mice (V. Makarov, unpubl. data), strongly suggesting that one or more nitroreductases, either mammalian or from the intestinal microbial flora, could carry out such a conversion. Indeed, it is well known that nitroaromatic compounds can be converted into their metabolites in the intestine, by the action of several microbial nitroreductases (Roldán *et al*., 2008). For instance, nitroreductase activity on 3-nitrobenzanthrone has been observed in several mouse tissues, mainly liver, lung, colon and bladder (Chen *et al*., 2008). In some cases microbial and mammalian NRs can compete for the same substrate: as an example, the anti-cancer pro-drug 5-(Aziridin-1-yl)-2,4-dinitrobenzamide (CB 1954) currently under clinical trials, can be activated by *E. coli* NfsB as well as in the liver, where cytochrome P450 reductase and NAD(P)H quinone oxidoreductase are involved, generating adverse hepatic effects (Tang *et al*., 2007). Interestingly, the activity of NfsB towards dinitrobenzamide pro-drugs raises the question of whether NfnB, or other mycobacterial NR, could reduce the new dinitrobenzamide compounds (Christophe *et al*., 2009) with antimycobacterial activity to the corresponding *amino*-derivatives, that, similarly to the BTZs derivatives, have been shown to be totally inactive (data not shown). Knowledge of the NfnB structure and the proposed complex with BTZ will help the rational design of second generation BTZ or dinitrobenzamides that are less susceptible to nitroreduction, thereby improving the half-life of the compounds and increasing their *in vivo* efficacy.

Experimental procedures

Standard microbiological and molecular biological procedures are described in the Supporting Information.

High pressure liquid chromatography analysis of BTZ conversion

Mycobacterium smegmatis mc^2155 and GM22 mutant strains were cultivated, as previously described, in 100 ml of com-

plete 7H9 broth and grown for 24 h. Then, 5 mg of BTZ043 was added to each 100 ml sample, and cultivated at 37°C for 1 or 3 h. After this period of time, each culture was quickly chilled, centrifuged at 3000 *g* and filtered through a 2 μm size filter.

Mycobacterium tuberculosis H37Rv strain was cultivated, as previously described, in 100 ml of complete 7H9 broth supplemented with ADC and grown for 72 h. Then, 5 mg of BTZ043 was added to each 100 ml sample, and cultivated at 37°C for 6, 18 or 72 h. After this period of time, each culture was quickly chilled, centrifuged at 3000 *g* and filtered through a 2 μm size filter.

In all cases the medium was diluted by 100 ml of water and extracted by chloroform for 3 times. Chloroform was evaporated in vacuum and residue was dissolved in 0.5 ml of acetonitrile. This solution was analysed by HPLC, to determine the concentrations of BTZ043 and BTZ045 compounds. Medium without drug was extracted in parallel, and used as control. Each experiment was performed 3 times. The data shown are the mean value obtained.

The HPLC conditions were as follow: HPLC system – 'Varian' with pumps ProStar 210, autosampler ProStar 410, UV detector ProStar 325 (wave 240 nm). Column 'Varian', Polaris C8-A, 3μ, 150 × 2.1 mm. The eluent is 0.1% formic acid in acetonitrile: 0.1% formic acid in water (50:50). Thermostat 20.0°C. Column flow 0.900 ml min^{-1}. Volume of injected probe (injector Rheodyne, loop) – 20 μl. Retention time of BTZ043 is 5.65 min and amino metabolite BTZ045 is 4.33 min.

Expression and purification of recombinant NfnB

In order to express a His-tagged fusion protein (His_6·NfnB), *nfnB* gene was PCR amplified from REP3 cosmid by using the 28nfnF and 28nfnR primers (Table S2). The 704 bp PCR product was cloned into pET-28a vector. The recombinant expression plasmid *nfnB*/pET-28a was used to transform *E. coli* BL21(DE3) and cells were plated onto LB agar containing kanamycin. The inoculum, grown at 37°C with kanamycin, was diluted 1:100 in 1 l of the same medium. The culture was incubated at 37°C until cells grew to OD_{600} = 0.5; then protein expression was induced with 1 mM isopropyl-β-thiogalactopyranoside (IPTG) for 2 h at 37°C. *E. coli* cells were resuspended in lysis buffer (50 mM NaH_2PO_4, 1.5 M NaCl, 5 mM β-mercaptoethanol and 10 mM imidazole, pH 7.9), and the following reagents were added to the lysate: 1 mg ml^{-1} lysozyme, 5 μg ml^{-1} DNase and 10 μg ml^{-1} RNase; the mixture was incubated on ice for 30 min and then sonicated. The cytosolic fraction was added to a Ni-nitrilotriacetic acid (Ni–NTA) resin (Qiagen), pre-equilibrated with lysis buffer in the absence of β-mercaptoethanol. The protein was eluted with 50 mM NaH_2PO_4, 1.5 M NaCl, 5 mM β-mercaptoethanol, 10% glycerol and 200 mM imidazole, pH 7.9. The fractions containing the NfnB protein, detected by SDS-PAGE, were collected and dialysed overnight at 4°C against 1 l of dialysis buffer (50 mM MOPS, 5 mM β-mercaptoethanol, 10 mM $MgCl_2$ and 10% glycerol, pH 7.9), and used for enzymatic assay. Purified NfnB was pooled and stored at –20°C.

Liquid chromatography – mass spectrometry (LC-MS) evaluation of BTZ conversion

The pretreatment reaction mixtures in the final volume of 50 μl described in the *Supporting information* were stopped by the same volume of acetonitrile and centrifuged at 14 000 *g* 10 min at room temperature. Ten microlitres of the sample was analysed by LC-MS method using LC-IT-TOF MS analyser (Shimadzu, Kyoto, Japan) with electrospray ionization (ESI) in the positive and negative mode. Ascentis C18 column (100 mm × 2.1 mm; 5 μm particles) was used for the separation. Elution of the compounds was performed by two-component gradient (H_2O:acetonitrile) (0–1 min – 10% acetonitrile, 5 min – 90% acetonitrile, 6 min – 90% acetonitrile, 6.01–12 min – 10% acetonitrile) with the flow rate of 0.2 ml min^{-1}. Identity of the individual peaks was confirmed by $MS\text{-}MS^3$ spectra.

Expression and purification of recombinant selenomethionyl substituted NfnB

In order to express His_6·NfnB fused to the TEV-protease recognition site, the *nfnB* gene was PCR amplified from REP3 by using the TEVnfnBf and TEVnfnBr oligonucleotides; the forward primer contained a sequence coding for the TEV-protease recognition site ENLYFQG (Table S2). The recombinant expression plasmid *nfnB*_TEV/pET-28a was used to transform *E. coli* B834(DE3). All transformants were used to inoculate LB containing kanamycin, and grown overnight at 30°C. Pre-inoculum was diluted 1:50 in M9 supplemented broth. The culture was incubated at 30°C until cells grew to OD_{600} = 1.0; then protein expression was induced with 1 mM IPTG for 24 h at 15°C and harvested. *E. coli* cells were resuspended in lysis buffer (50 mM NaH_2PO_4, 0.5 M NaCl, 5% glycerol and 25 mM imidazole, pH 8.0), supplemented with Complete protease inhibitor cocktail (Roche); the mixture was then sonicated. The lysate was centrifuged at 26 800 *g* for 1 h, filtered (0.45 μm) and loaded onto a 1 ml His Trap Ni^{2+} ± IMAC column (GE Healthcare) equilibrated in lysis buffer; the recombinant protein was purified by a linear imidazole gradient (25–400 mM). The fractions containing the SeMet–NfnB protein were checked by 15% SDS-PAGE, collected, and dialysed overnight at 4°C against 1 l of 50 mM Tris-HCl, 150 mM NaCl, 5% glycerol, 1 mM dithiothreitol pH 8.0, in the presence of His_6-tagged TEV protease (van den Berg *et al.*, 2006), at a ratio of 1:30 (w/w). SeMet–NfnB was separated both from His-tag and the protease, using Ni–NTA affinity chromatography by gravity flow. The untagged SeMet–NfnB was successively purified by size-exclusion chromatography on a Superdex 200 26/60 column (GE Healthcare) equilibrated in 50 mM Tris-HCl, 150 mM NaCl, 5% glycerol, pH 8.0. Fractions corresponding to the SeMet–NfnB peak were concentrated up to 37 mg ml^{-1} with a 10 kDa cut-off Vivaspin concentrator (Sartorius). The protein concentration was determined by Bradford assay, and the purity estimated about 95%, by SDS-PAGE and Coomassie blue staining. The SeMet–NfnB solution was pooled, flash-frozen in liquid nitrogen, and stored at –80°C.

Enzymatic assays

The activity of *M. smegmatis* NfnB was determined with an assay mixture containing NAD(P)H ranging from 5 to 100 μM,

in 1.0 ml 50 mM Tris-HCl, 150 mM NaCl, 5% glycerol, pH 8.0. The reaction was started by addition of 3 μM purified NfnB, and the activity was determined at 25°C from the linear decrease in adsorbance at 340 nm, following NAD(P)H oxidation. As internal control the activity of *E. coli* nitroreductase (Sigma-Aldrich) was determined as well.

Crystallization

Crystals of NfnB were obtained from a stock solution (35 mg ml^{-1}) of selenomethionyl protein via sitting-drop vapour diffusion at 18°C, by mixing equal volumes (1 μl) of enzyme solution, supplemented with 1 mM FMN, with 20% (w/v) PEG8000, 6% (v/v) isopropanol, 200 mM $NH_4H_2PO_4$. To obtain crystals of the protein in complex with the NADPH cofactor, 5.8 mM NADPH was added to the enzyme prior to crystallization. Rod-shaped crystals appeared after 3 days and reached their maximum dimension over 2–3 weeks. Prior to data collection, crystals were flash-cooled in liquid nitrogen after a soaking into a cryoprotectant solution made of 75% mother liquor and 25% glycerol.

Data collection, structure solution and refinement

X-ray diffraction data were collected either at the Proxima-1 beamline at the Soleil Synchrotron (Saint-Aubin, France) or the microfocus ID23-2 beamline at the ESRF (Grenoble, France) from single crystals at 100 K. A 2.5 Å resolution dataset was collected from a single selenomethionyl crystal at the X-ray energy corresponding to the peak of the selenium K-edge (12.664 keV, $\lambda = 0.9790$ Å), as measured by a fluorescence scan. Treatment of diffraction images was carried out with either XDS (Kabsch, 1993) or MOSFLM from the CCP4 suite (Collaborative Computational Project, Number 4, 1994), followed by data reduction with SCALA (Collaborative Computational Project, Number 4, 1994) (Table 6). A total of 12 selenium sites were located with the program SHELXD (Sheldrick, 2008), and single-wavelength anomalous diffraction (SAD) phasing and density modification were carried out with AutoSHARP (Vonrhein *et al.*, 2007). The resulting solvent-flipped electron density map showed clear secondary structure features and allowed the manual tracing of the polypeptide chain with Coot (Emsley and Cowtan, 2004). The model was initially refined with phenix.refine (Adams *et al.*, 2010), then with BUSTER (Blanc *et al.*, 2004) against 1.75 Å resolution data collected from an isomorphous selenomethionyl crystal. Diffraction data of the isomorphic NADPH complex were collected at 1.85 Å resolution and the structure refined starting from the co-ordinates of the native enzyme. TLS groups were defined with the TLSMD server (http://skuld.bmsc.washington.edu/~tlsmd) (Painter and Merritt, 2006). Both models were validated through the Molprobity server (http://molprobity.biochem.duke.edu) (Davis *et al.*, 2007). Final refinement parameters are shown in Table 6. Figures were generated and rendered with Pymol (http://www.pymol.org); electrostatic surfaces were rendered with the APBS plugin within Pymol, supplying atomic charges and radii calculated through the 'pdb2pqr' server (http://www.poissonboltzmann.org/pdb2pqr/) (Dolinsky *et al.*, 2004) applying the CHARMM force field. Atomic co-ordinates and structure factors have been deposited in the protein data bank, with accession codes 2WZV (highest resolution) and 2WZW (NADPH complex).

Docking

The docking procedure for both NADPH and the BTZ043 molecules was entirely carried out with the Icm software (Totrov and Abagyan, 1997). Prior to any calculation, all solvent molecules were removed, hydrogens added and the hydrogen bond network optimized. Exploration of the NfnB surface was carried out with IcmPocketFinder to identify suitable pockets for docking (An *et al.*, 2004). Residues closer than 2.5 Å to the binding pocket were considered to mark the boundary of the 5 grid potentials required by Icm to describe interactions of the flexible ligand with the receptor. Solutions were ranked according to their predicted binding energy, and the predicted complex (lowest free energy) was minimized with Szybki (http://www.eyesopen.com), considering the Poisson-Bolzmann electrostatic potential, solvation terms and the flexibility of both the ligand and the active site residues of the enzyme.

Acknowledgements

The expression plasmid for recombinant TEV protease was kindly provided by H. Berglund (Karolinska Institute, Stockholm). We are grateful to P. Weber (PF6, Institut Pasteur) for performing robot-driven crystallization trials, P. Schneider for technical assistance, and Dr J. McKinney for plasmid pJG1100. We thank ESRF and Soleil for granting access to synchrotron radiation facilities and their staff for the onsite assistance. João Neres is the recipient of a Marie Curie fellowship from the European Commission. LC-MS analyses were performed with the support of Slovak Research and Development Agency No. VVCE-0070-07 and grant of Slovak Grant Agency no. 1/0546/10. This work was funded by EC-VI Framework Contract No. LSHP-CT-2005-018923.

References

Adams, P.D., Afonine, P.V., Bunkóczi, G., Chen, V.B., Davis, I.W., Echols, N., *et al.* (2010) PHENIX: a comprehensive Python-based system for macromolecular structure solution. *Acta Crystallogr D* **66:** 213–221.

An, J., Totrov, M., and Abagyan, R. (2004) Comprehensive identification of ″druggable″ protein ligand binding sites. *Genome Inform* **15:** 31–41.

van den Berg, S., Lofdahl, P.A., Hard, T., and Berglund, H. (2006) Improved solubility of TEV protease by directed evolution. *J Biotechnol* **121:** 291–298.

Blanc, E., Roversi, P., Vonrhein, C., Flensburg, C., Lea, S.M., and Bricogne, G. (2004) Refinement of severely incomplete structures with maximum likelihood in BUSTER-TNT. *Acta Crystallogr D* **60:** 2210–2221.

Chen, G., Gingerich, J., Soper, L., Douglas, G.R., and White, P.A. (2008) Tissue-specific metabolic activation and mutagenicity of 3-Nitrobenzanthrone in Muta™Mouse. *Environ Mol Mutagen* **49:** 602–613.

Christophe, T., Jackson, M., Jeon, H.K., Fenistein, D., Contreras-Dominguez, M., Kim, J., *et al*. (2009) High content screening identifies decaprenyl-phosphoribose 2′ epimerase as a target for intracellular antimycobacterial inhibitors. *PLoS Pathog* **5:** e10000645.

Collaborative Computational Project, Number 4 (1994) The CCP4 suite: programs for protein crystallography. *Acta Crystallogr D* **50:** 760–763.

Davis, I.W., Leaver-Fay, A., Chen, V.B., Block, J.N., Kapral, G.J., Wang, X., *et al*. (2007) MolProbity: all-atom contacts and structure validation for proteins and nucleic acids. *Nucleic Acids Res* **35:** W375–W383.

Dolinsky, T.J., Nielsen, J.E., McCammon, J.A., and Baker, N.A. (2004) PDB2PQR: an automated pipeline for the setup of Poisson-Boltzmann electrostatics calculations. *Nucleic Acids Res* **32:** W665–W667.

Emsley, P., and Cowtan, K. (2004) Coot: model-building tools for molecular graphics. *Acta crystallogr D* **60:** 2126–2132.

Haynes, C.A., Koder, R.L., Miller, A.F., and Rodgers, D.W. (2002) Structures of nitroreductase in three states. Effects of inhibitor binding and reduction. *J Biol Chem* **277:** 11513–11520.

Holm, L., Kaariainen, S., Rosenstrom, P., and Schenkel, A. (2008) Searching protein structure databases with DaliLite v.3. *Bioinformatics* **24:** 2780–2781.

Johansson, E., Parkinson, G.N., Denny, W.A., and Neidle, S. (2003) Studies on the nitroreductase prodrug-activating system. Crystal structures of complexes with the inhibitor dicoumarol and dinitrobenzamide prodrugs and of the enzyme active form. *J Med Chem* **46:** 4009–4020.

Kabsch, W. (1993) Automatic processing of rotation diffraction data from crystals of initially unknown symmetry and cell constants. *J Appl Crystallogr* **26:** 795–800.

Krissinel, E., and Henrick, K. (2004) Secondary-structure matching (SSM), a new tool for fast protein structure alignment in three dimensions. *Acta Crystallogr D* **60:** 2256–2268.

Linwu, S.W., Syu, C.J., Chen, Y.L., Wang, A.H., and Peng, F.C. (2009) Characterization of *Escherichia coli* nitroreductase NfsB in the metabolism of nitrobenzodiazepines. *Biochem Pharmacol* **78:** 96–103.

Lovering, A.L., Hyde, E.I., Searle, P.F., and White, S.A. (2001) The structure of *Escherichia coli* nitroreductase complexed with nicotinic acid: three crystal forms at 1.7 Å, 1.8 Å and 2.4 Å resolution. *J Mol Biol* **309:** 203–213.

Maartens, G., and Wilkinson, R.J. (2007) Tuberculosis. *Lancet* **370:** 2030–2043.

Makarov, V., Manina, G., Mikusova, K., Möllmann, U., Ryabova, O., Saint-Joanis, B., *et al*. (2009) Benzothiazinones kill *Mycobacterium tuberculosis* by blocking arabinan synthesis. *Science* **324:** 801–804.

Manjunatha, U.H., Boshoff, H., Dowd, C.S., Zhang, L., Albert, T.J., Norton, J.E., *et al*. (2006) Identification of a nitroimidazo-oxazine-specific protein involved in PA-824 resistance in *Mycobacterium tuberculosis*. *Proc Natl Acad Sci USA* **103:** 431–436.

Marcinkeviciene, J., and Blanchard, J.S. (1997) Catalytic properties of lipoamide dehydrogenase from *Mycobacterium smegmatis*. *Arch Biochem Biophys* **340:** 168–176.

Matteelli, A., Migliori, G.B., Cirillo, D., Centis, R., Girard, E., and Raviglione, M. (2007) Multidrug-resistant and extensively drug-resistant *Mycobacterium tuberculosis*: epidemiology and control. *Expert Rev Anti Infect Ther* **5:** 857–871.

Mikusova, K., Huang, H., Yagi, T., Holsters, M., Vereecke, D., D'Haeze, W., *et al*. (2005) Decaprenylphosphoryl arabinofuranose, the donor of the *d*-arabinofuranosyl residues of mycobacterial arabinan, is formed via a two-step epimerization of decaprenylphosphoryl ribose. *J Bacteriol* **187:** 8020–8025.

Painter, J., and Merritt, E.A. (2006) Optimal description of a protein structure in terms of multiple groups undergoing TLS motion. *Acta Crystallogr D* **62:** 439–450.

Parish, T., and Stoker, N.G. (2000) Use of a flexible cassette method to generate a double unmarked *Mycobacterium tuberculosis tlyA plcABC* mutant by gene replacement. *Microbiology* **146:** 1969–1975.

Parkinson, G.N., Skelly, J.V., and Neidle, S. (2000) Crystal structure of FMN-dependent nitroreductase from *Escherichia coli* B: a prodrug-activating enzyme. *J Med Chem* **43:** 3624–3631.

Pasca, M.R., Degiacomi, G., De Jesus Lopes Ribeiro, A.L., Zara, F., De Mori, P., Heym, B., *et al*. (2010) Clinical isolates of *Mycobacterium tuberculosis* in four european hospitals are uniformly susceptible to benzothiazinones. *Antimicrob Agents Chemother* **54:** 1616–1618.

Purkayastha, A., McCue, L.A., and McDonough, K.A. (2002) Identification of a *Mycobacterium tuberculosis* putative classical nitroreductase gene whose expression is coregulated with that of the *acr* gene within macrophages, in standing versus shaking cultures, and under low oxygen conditions. *Infect Immun* **70:** 1518–1529.

Race, P.R., Lovering, A.L., Green, R.M., Ossor, A., White, S.A., Searle, P.F., *et al*. (2005) Structural and mechanistic studies of *Escherichia coli* nitroreductase with the antibiotic nitrofurazone. Reversed binding orientations in different redox states of the enzyme. *J Biol Chem* **280:** 13256–13264.

Riccardi, G., Pasca, M.R., and Buroni, S. (2009) *Mycobacterium tuberculosis*: drug resistance and future perspectives. *Future Microbiol* **4:** 597–614.

Roldán, M.D., Pérez-Reinado, E., Castillo, F., and Moreno-Vivián, C. (2008) Reduction of polynitroaromatic compounds: the bacterial nitroreductases. *FEMS Microbiol Rev* **32:** 474–500.

Sassetti, C.M., Boyd, D.H., and Rubin, E.J. (2003) Genes required for mycobacterial growth defined by high density mutagenesis. *Mol Microbiol* **48:** 77–84.

Sheldrick, G.M. (2008) A short history of SHELX. *Acta Crystallogr A* **64:** 112–122.

Singh, R., Manjunatha, U., Boshoff, H.I., Ha, Y.H., Niyomrattanakit, P., Ledwidge, R., *et al*. (2008) PA-824 kills nonreplicating *Mycobacterium tuberculosis* by intracellular NO release. *Science* **322:** 1392–1395.

Stover, C.K., Warrener, P., VanDevanter, D.R., Sherman, D.R., Arain, T.M., Langhorne, M.H., *et al*. (2000) A small-molecule nitroimidazopyran drug candidate for the treatment of tuberculosis. *Nature* **405:** 962–966.

Tang, M.H., Helsby, N.A., Goldthorpe, M.A., Thompson, K.M., Al-Ali, S., and Tingle, M.D. (2007) Hepatic nitroreduction, toxicity and toxicokinetics of the anti-tumour prodrug CB 1954 in mouse and rat. *Toxicology* **240:** 70–85.

Totrov, M., and Abagyan, R. (1997) Flexible protein-ligand

docking by global energy optimization in internal coordinates. *Proteins* **29** (Suppl. 1)**:** 215–220.

Vonrhein, C., Blanc, E., Roversi, P., and Bricogne, G. (2007) Automated structure solution with autoSHARP. *Methods Mol Biol* **364:** 215–230.

Wolucka, B.A. (2008) Biosynthesis of *d*-arabinose in mycobacteria – a novel bacterial pathway with implications for antimycobacterial therapy. *FEBS J* **68:** 2602–2613.

Zenno, S., Koike, H., Kumar, A.N., Jayaraman, R., Tanokura, M., and Saigo, K. (1996) Biochemical characterization of NfsA, the *Escherichia coli* major nitroreductase exhibiting a high amino acid sequence homology to Frp, a *Vibrio harveyi* flavin oxidoreductase. *J Bacteriol* **178:** 4508–4514.

Supporting information

Additional supporting information may be found in the online version of this article.

Please note: Wiley-Blackwell are not responsible for the content or functionality of any supporting materials supplied by the authors. Any queries (other than missing material) should be directed to the corresponding author for the article.